Pergamon

Journal of Structural Geology, Vol. 18, Nos 2/3, pp. 199 to 214, 1996

0191-8141/96 $15.00 + 0.00

0191-8141(95)00106-9

Scaling systematics of fault sizes on a large-scale range fault map

J. WATTERSON, J. J. WALSH, P. A. GILLESPIE and S. EASTON

Fault Analysis Group, Department of Earth Sciences, University of Liverpool, Liverpool L69 3BX, U.K.

(*Received* 9 *January* 1995; *accepted in revised form* 21 *August* 1995)

Abstract—A large-scale, high-quality fault map was produced for an intensively mined area of the U.K. South Yorkshire coalfield. This database has been used to investigate both the scaling properties of fault systems and the robustness of techniques for the prediction of sub-resolution faulting. The mapped area is 87 km^2 and contains 2257 individual fault traces with, on average, one throw reading available for every 82 m of fault trace; recorded throw values range from 10 cm to 180 m and fault trace lengths from 10 m to 12 km. Two sets of normal faults (NW- and NE-striking) are present, together with local WNW-striking dextral strike-slip zones.

Size populations are power-law over at least 2.5 orders of magnitude and the exponents of the throw, maximum throw and fault trace length population curves are interrelated and, taking into account the effects of resolution on trace length populations, are internally consistent. Derivatives of the primary map reproduce resolutions typical of offshore seismics and illustrate the limitations of seismic data. Power-law fault size distributions provide a basis for sub-seismic fault prediction. For this data set, a fault throw resolution of better than 10 m would be required to provide an accurate prediction of the throw population down to *ca* 0.6 m.

INTRODUCTION

Investigation of the scaling properties and other systematics of fault systems requires high-quality fault data. In this context quality is primarily a function of the range of fault sizes represented, the degree to which faults within the nominal size range are fully represented, the amount of available fault displacement (or throw) data and the size of area mapped in relation to the sizes of the faults. An intensively mined 87 km^2 area of the East Pennine coalfield in South Yorkshire, U.K., was chosen as likely to provide the amount and quality of data needed for construction of such a map (Fig. 1). The mapped coal seams lie within the Carboniferous Westphalian deltaic sequence of the East Pennine Coalfield (Goossens & Smith 1973). Faulting is mainly post-Westphalian and pre-Permian and comprises an orthogonal system of NE- and NW-striking normal faults, with throws of up to 180 m, post-dated by two WNW dextral strike-slip fault zones (Fig. 2a). Because this map incorporates a wide range of fault sizes, it provides a basis for detailed examination of the density and size distributions of faults and of the effects of data resolution on fault data sets: consideration of the spatial distributions of faults will be presented elsewhere.

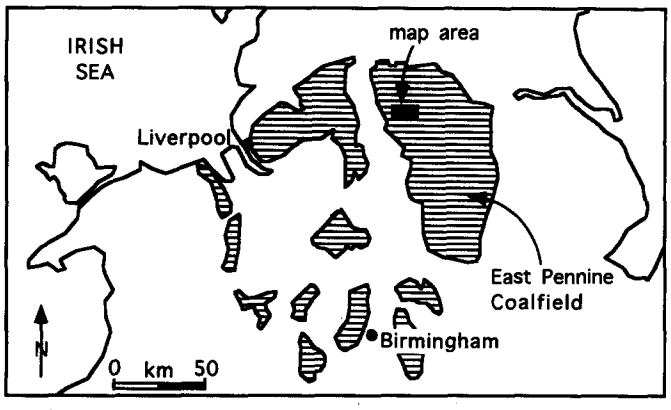

Fig. 1. Map showing location of map area and principal areas of exposed and concealed coalfields (dark shading).

The mapped area has been mined, often by multi-seam workings, to an extent which offered the prospect of almost complete areal coverage by combining data from several worked seams. For most of the century it has been a legal requirement that 'seam abandonment plans' be drawn up and archived with the relevant authority for all workings in which coaling has been completed. For most of this time abandonment plans have been submitted on a scale of 1:2500. Among the features represented on the plans are boundaries of workings, seam 'levels' (i.e. elevations), fault traces and throw values at intervals along the fault traces. For throws up to approximately the thickness of a worked seam (<*ca* 3 m), the recorded throw values are those which were measured in the workings, and for larger throws, the values are those calculated from the offsets of the seam elevation contours derived from the levelling data. Minimum recorded fault throws are 10 cm (formerly, 6 inches) and other throw values are sometimes given to the nearest 5 cm or 3 inches.

An attraction of coal mine fault data is that they include a size range of faults which bridges the gap between the scale ranges of outcrop fault data on the one hand and oilfield seismic survey fault data on the other. The initial impetus for this work was the need, as perceived at that time, to develop methods for prediction of the numbers and locations of sub-seismic faults for application in planning new coal mines. For coal seams at typical U.K. working depths, 300–400 m, surface seismic data can, at best, image fault throws down to *ca* 5 m; but, depending on seam thickness, faults with throws of as little as *ca* 1 m may impede mechanized

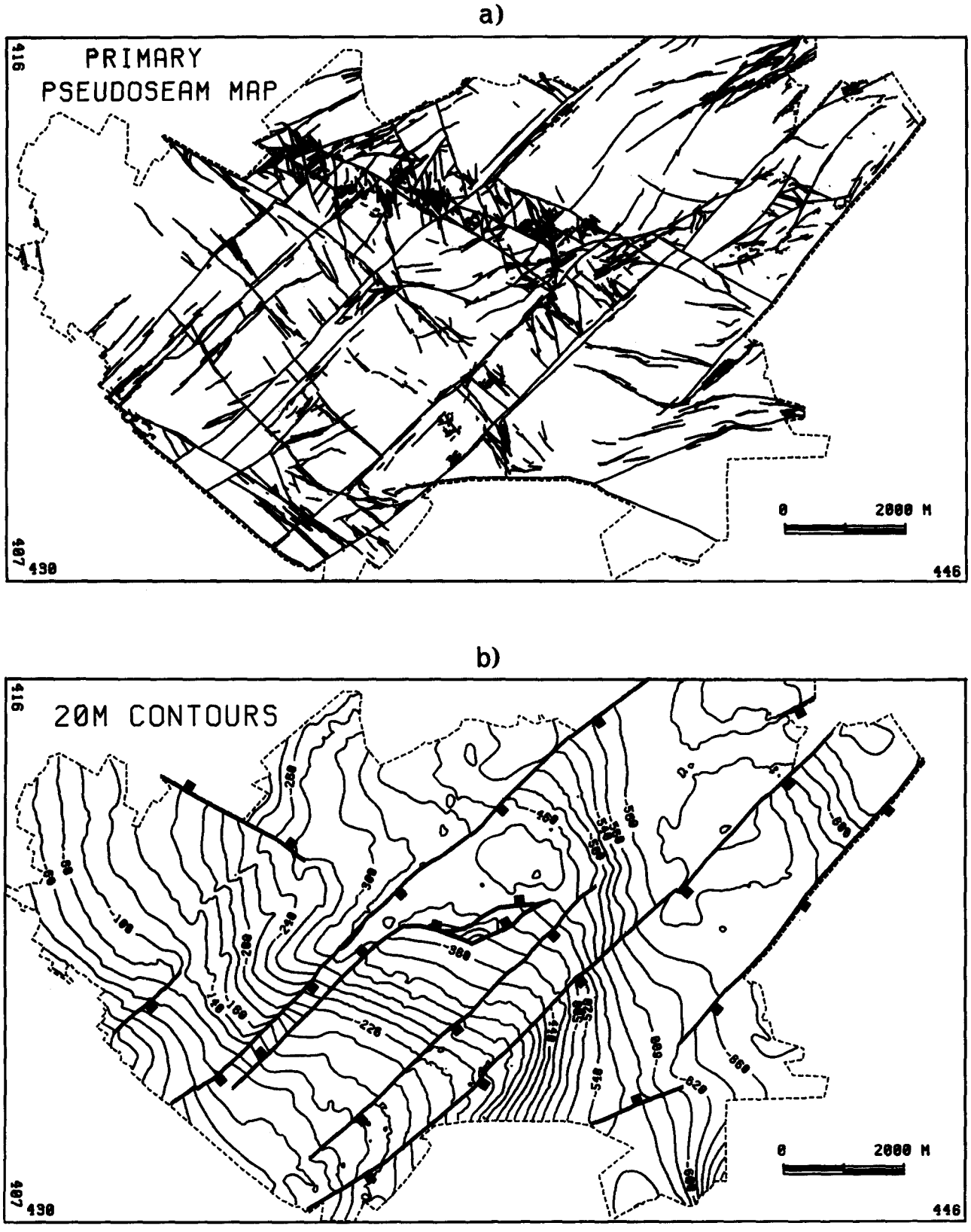

Fig. 2. (a) Primary pseudoseam map showing all mapped fault traces and boundary of mapped area (broken line). Location shown by National Grid References of N–S and E–W frame lines. (b) Structural contours on pseudoseam with 20 m contour interval. Only fault traces with throws ≥20 m are shown.

retreat longwall mining. There is a comparable difficulty in the structural characterization of hydrocarbon reservoirs in which sub-seismic faults may have a pronounced effect on fluid flow, especially where the reservoir interval thickness is the same as, or even less than, the smallest seismically-imaged fault throws. The smallest fault throws of concern vary with the reservoir interval thickness, the sand–shale distribution and the hydraulic properties of the fault surfaces: if fault surfaces are barriers to flow, then throws of as little as 1 m may be

significant because a 1 m fault may extend for more than 100 m both up and down dip and extend laterally for a minimum of 200 m in both directions. At reservoir depths in the North Sea the seismic vertical resolution, or fault detectability limit, is rarely as good as 20 m and may exceed 50 m. Fault maps based on coal seam data therefore include the size range of faults intermediate between that seismically imaged offshore and that represented in core or borehole-image data. The size range of faults recorded in coal mine data is also that which is relevant to some hydrogeological and hazardous waste storage problems. More generally, the extended scale range of faults recorded in coal mine data provides a firmer basis for theoretical investigation of fault systematics than is afforded by most other types of fault data.

CONSTRUCTION AND QUALITY ASSESSMENT OF THE FAULT MAP

Database

Abandonment plans for 12 coal seams (Table 1) were examined and their quality assessed in terms of areal coverage of workings, age of workings and completeness of fault and levelling data. Workings from the 1950s and 1960s provide the best data because the standard of data recording was high and the mining methods then in use allowed economic working even of heavily faulted areas. Substantial effort has been devoted to editing of the data and filling of gaps between workings either by lateral interpolation or extrapolation of data or by vertical extrapolation from other seams, using the methods described by Walsh & Watterson (1990). Only six seams (Table 1), all within a vertical interval of 148 m, provide sufficient coverage for inclusion in the initial database but information from other seams was used to make, or to validate, the interpolations and extrapolations necessary to fill gaps in the coverage of the six selected seams.

Table 1. Seams examined for construction of the primary fault map showing heights relative to the Top Haigh Moor seam. The pseudoseam map was generated from seam elevation and fault data mainly from three seams (underlined) but fault data from adjacent seams (*) were incorporated by extrapolation and interpolation to infill otherwise unworked ground. Data from the remaining seams were used principally for analysis of fault dips

Seam	Vertical distance from Top Haigh Moor (m)
Kents Thick	127
Top Softs	80
Barnsley	68
Dunsil*	52
Haigh Moor*	14
Top Haigh Moor	0
Lidgett	−32
Flockton Thick*	−79
Flockton Thin	−98
Deep Hard	−114
Parkgate	−145
Thorncliffe	−160

Data from the six seams were digitized using a conventional commercial mapping package. The data types included in the initial database are: boundaries of worked panels, roadways, levels, shaft locations, seam elevations and faults. Fault traces are recorded in centre-line format together with associated throw values and throw directions. Fault trace data are recorded and flagged according to type and quality (see below) and the terminations of fault traces labelled as either 'tip-point' or 'end of data'.

Primary fault map

The intention was to construct a single 'pseudoseam' map (Fig. 2a) for as large a contiguous area as possible by projecting data from actual seams upwards or downwards to the pseudoseam level, using mainly data from three seams (Lidgett, Top Haigh Moor and Barnsley) which all occur within a vertical interval of *ca* 100 m (Table 1). Investigation of a range of polynomial fits of the height data showed that a satisfactory pseudoseam could be constructed at Top Haigh Moor level with a static shift of +32 m for the Lidgett and −68 m for the Barnsley seam. These shifts maintain both the local topographies of the seams and a consistent regional structure (Fig. 2b). The principal problem arising from a simple vertical shift is the resulting lateral offset of traces of non-vertical faults which gives rise to fault trace discontinuities at boundaries between areas of data derived from different seams. Such discontinuous traces were linked during construction of the pseudoseam map; this procedure does not significantly affect the statistical properties of the map because the linkages needed are very short, due to the small vertical intervals between the seams and the relatively steep dips of normal faults (mean dip = 69°). The *primary pseudoseam* map (Figs. 2a and 3) has an area of 87 km^2 with 2257 individual fault traces and with 6953 throw values and 23,555 levelling values recorded. One throw reading is available on average for every 82 m of fault trace but 445 fault traces have no attached throw reading mainly because they are small faults with trace lengths generally less than 200 m. A small part of a densely faulted part of the map area is shown in Fig. 4 at a scale which allows fault trace and throw data to be seen.

Quality assessment of the pseudoseam map

Analysis of geological data requires an explicit assessment of data quality and limitations. The style of archive seam-abandonment plans varies from one colliery to another and with the age of workings. A principal concern was to determine whether the apparent variation in fault density on the pseudoseam map is real or is the result of some systematic bias of the primary data. Although data from nine individual collieries are incor-

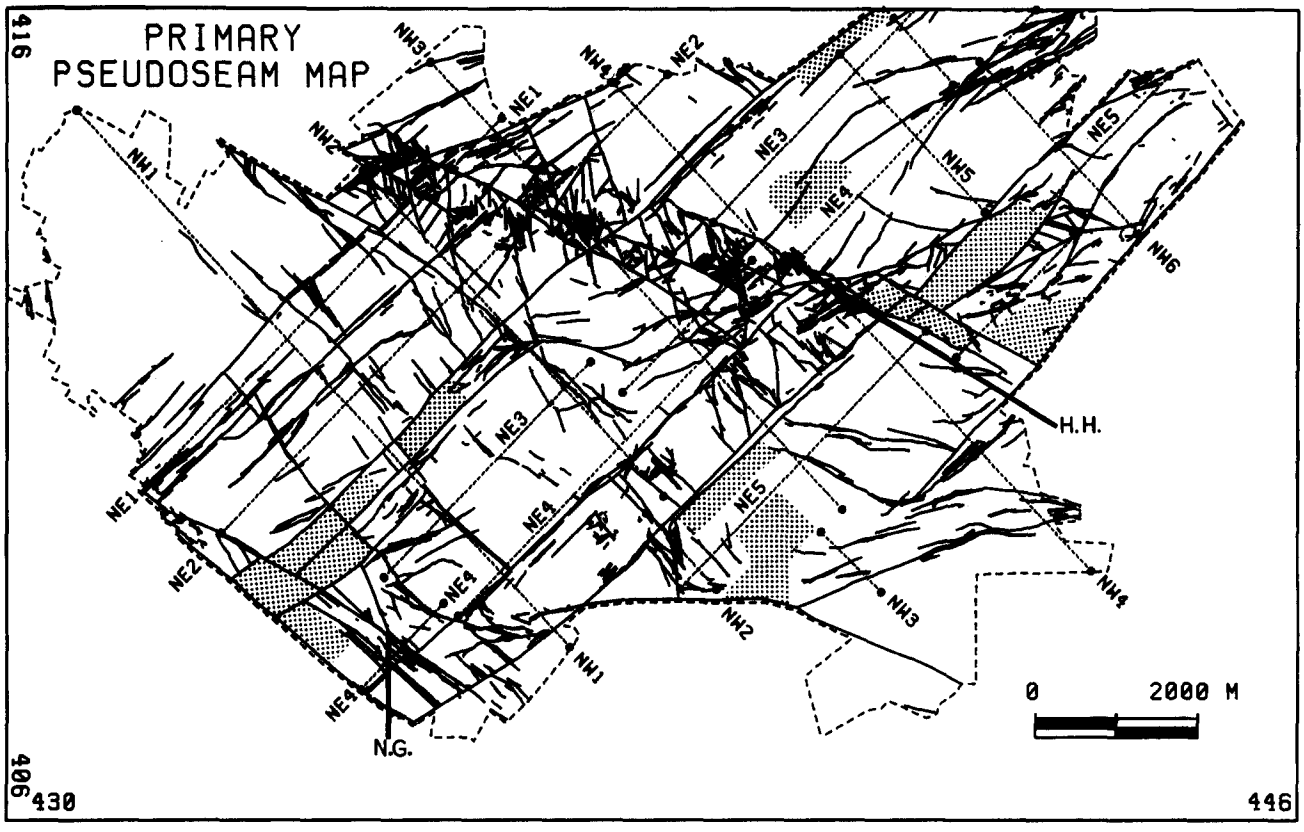

Fig. 3. Primary pseudoseam map showing all fault traces and sample lines (labelled). Areas of poor or no data within outer map boundary are shown stippled. Note that some sample lines are offset to avoid areas of poor data. The positions of the Holgate Hospital (H.H.) and North Gawber (N.G.) strike-slip fault zones are shown.

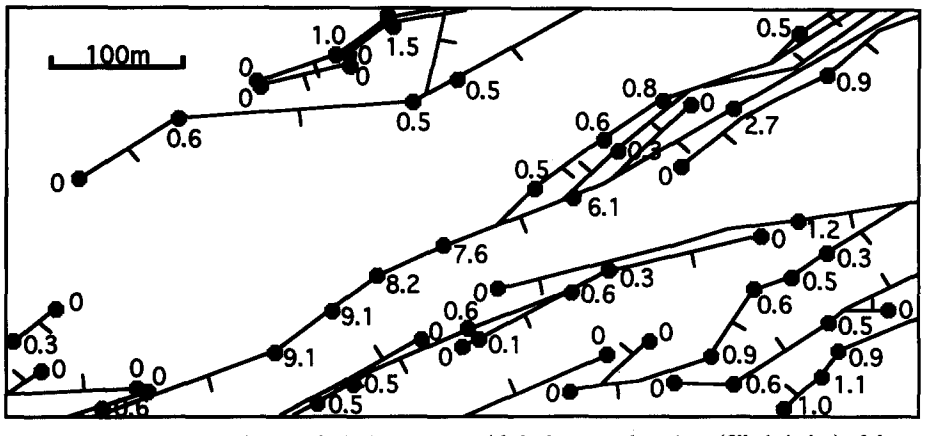

Fig. 4. Detail of pseudoseam map showing fault data output with fault traces, locations (filled circles) of throw values (m) and fault dip directions (ticks).

porated in the map, the boundaries of structurally distinct areas on the map do not coincide with colliery boundaries except where these coincide with a large fault, as often occurs. Similarly, variations in fault density within the map area appear to be unrelated to either the ages of workings or the mapped coal seam. Although older workings usually have relatively few levelling data, they do not coincide with low fault densities. More recent workings tend to be concentrated in less densely faulted areas because information from earlier workings was used to identify and avoid the more heavily faulted areas. Small areas for which there are no data are principally due to fluvial channels, where coal seams are absent (washouts), or to intense deformation in the hangingwalls of larger faults which has discouraged coal extraction. These phenomena are the principal cause of the indented boundary of the mapped area and for the areas of incomplete data identified in Fig. 3.

A crucial aspect of data quality is the lower limit of resolution, or truncation value. Fault tip-points which are shown on abandonment plans are known not to be points of zero throw but have throws of *ca* 10–15 cm. We take the resolution limit of a fault data set to be the smallest attribute value (e.g. throw or trace length) for which the map is complete, or nearly so, rather than the smallest value which is shown. Truncation values cannot

be determined simply by inspection of the pseudoseam map but are shown in a later section to be *ca* 60 cm for throw and *ca* 200 m for trace length. The range of throws believed to be fully represented on the map is 0.6–180 m (i.e. 2.48 decades) and the range of trace lengths is 0.2–12 km (i.e. 1.78 decades).

STRUCTURE OF THE MAP AREA

The structure within the map area is similar to that elsewhere in the Yorkshire coalfield. The regional bed dip is 3.5° NE and the structural complexity seen in Fig. 2(b) is due mainly to folding which accommodates the fault-related deformation (Gibson *et al.* 1989) and folds which post-date faulting (Goossens & Smith 1973). The fault pattern of the mapped area comprises an orthogonal system of NE- and NW-striking normal faults (Fig. 5) and two WNW-striking strike-slip fault zones, all of which are post-depositional, late- to post-Westphalian structures (Rippon 1985a,b, Walsh & Watterson 1988a). Faults of the dominant NE-striking normal fault set dip at 68° (mean dip of 15 faults measured from seam to seam), which compares with the mean 69° dip of dip-slip faults in the East Pennine coalfield (Walsh & Watterson 1988a), and the numbers of SE- and NW-dipping faults in this set are in the ratio *ca* 7:6, with the larger displacements on SE-dipping faults (Fig. 5). Faults of the subsidiary NW-striking set dip at 70° (mean dip of 13 faults) with NE- and SW-dipping faults in the ratio *ca* 7:5, with the larger displacements on NE-dipping faults (Fig. 5). Previous work shows that tectonic normal faults from the East Pennine Coalfield with sizes above the estimated truncation value of the pseudoseam map (e.g. 200 m trace length) will have a vertical extent greater than the vertical interval between the three main seams (>100 m) used to produce the pseudoseam map (Rippon 1985a,b, Walsh & Watterson 1988b, 1990).

Table 2. Numbers of intersections with fault traces for each of the sample lines incorporated in one-dimensional throw population data sets

NE sample lines	NE1	NE2	NE3	NE4	NE5		Total
Fault intersections	24	46	34	63	30		197
NW sample lines	NW1	NW2	NW3	NW4	NW5	NW6	Total
Fault intersections	28	34	61	48	7	29	207

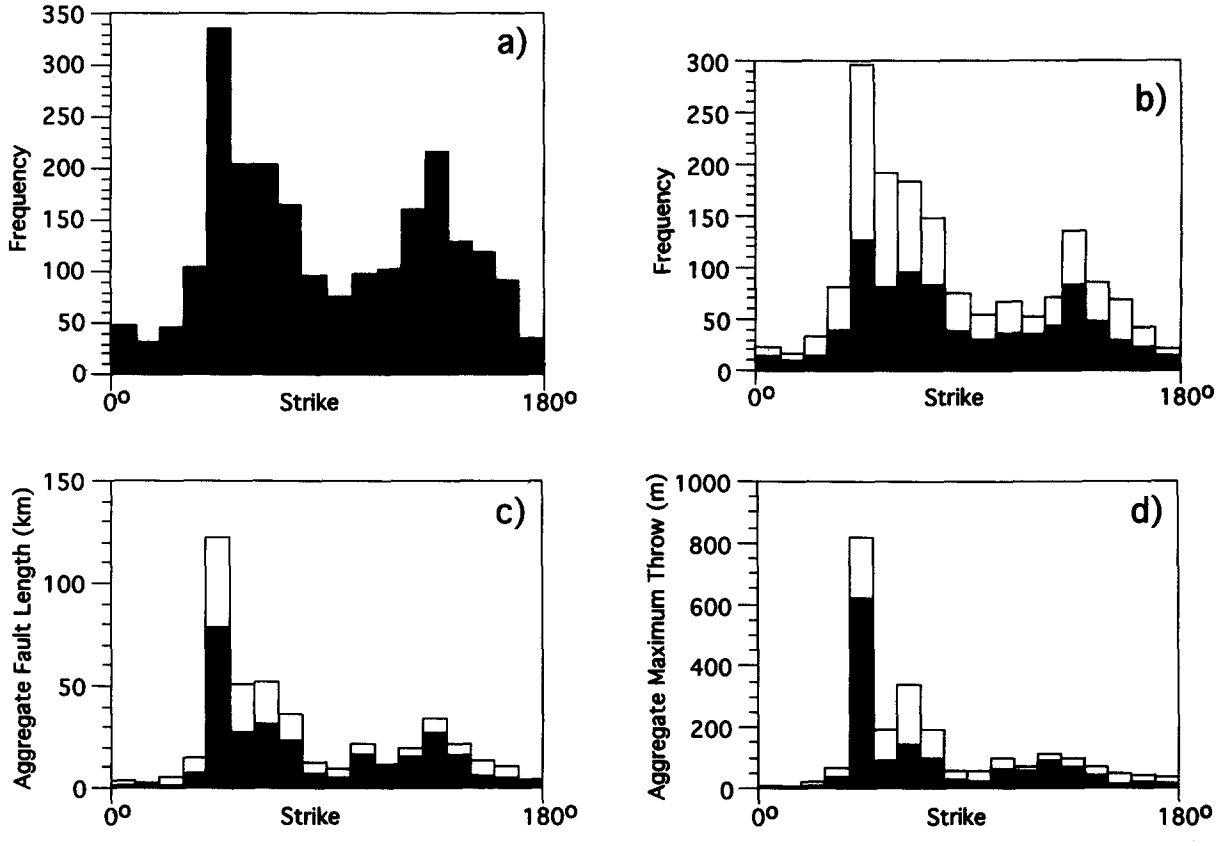

Fig. 5. Histograms of strike directions of faults on primary map. (a) All faults, including Holgate Hospital and North Gawber strike-slip fault zones. (b) Normal faults. (c) Histogram weighted by fault trace length for all normal faults. (d) Histogram weighted by maximum throw for all normal faults. Normal faults of either set with a westerly component of dip are shown white.

Compactional or gravity-slide syn-depositional faults which have a more limited vertical persistence (<50 m) do not occur within the principal seams of the study area although, locally, are quite common within the East Pennine Coalfield. No clear cross-cutting relationships can be established for the NE and NW normal fault sets, but the compartmentalization of smaller displacement NW faults between larger displacement NE faults is consistent with a later or, more likely, similar age. Elsewhere in the coalfield up to 25% but generally <10% of the displacement on large normal faults post-dates the unconformably overlying Permian sequence (our unpublished data and Elliott (National Coal Board internal report, *ca* 1954)). Two WNW strike-slip fault zones occur within the mapped area, the Holgate Hospital and North Gawber zones, which offset some of the earlier normal faults. The Holgate Hospital zone extends through the middle of the map area, is *ca* 1 km wide and comprises *ca* 500 faults with small dip-slip components of displacement. The Holgate Hospital fault *sensu stricto* is reported to have *ca* 140 m dextral strike-slip offset (Goossens & Smith 1973) but inspection of the new map suggests >300 m dextral offset on the Holgate Hospital strike-slip zone. Intense zones of minor faults are typically associated with strike-slip faulting of sub-horizontal bedded sequences because, unlike dip-slip faulting, the fault-related deformation cannot be accommodated by bedding-plane slip. The North Gawber strike-slip zone occurs in the extreme SW of the map area within the take of the North Gawber Colliery. All fault traces believed to be associated with the Holgate Hospital and North Gawber strike-slip zones are flagged in the database to allow their exclusion from some of the analyses. Northwest-striking strike-slip faults other than those associated with the identified Holgate Hospital and North Gawber strike-slip zones could occur within the map area but as the regional strike of strike-slip faults is 10–15° anti-clockwise of the NW normal faults, the NW fault set is unlikely to include strike-slip faults. The Holgate Hospital fault is parallel to the 4 km wide Morley–Campsall strike-slip fault zone which lies *ca* 10 km to the NE of the map area and is regarded by Graham (1988) as the dominant fault of the Yorkshire coalfield. The dip-slip component of the Morley–Campsall fault downthrows to the SW but the magnitude of neither dip-slip nor strike-slip component is known (Graham 1988). The strike-slip faults post-date the normal faults in this region but we have no other information regarding their age.

MAPS DERIVED FROM THE PRIMARY PSEUDOSEAM MAP

Derivatives of the primary pseudoseam fault map (Figs. 6a–f) have been obtained by 'clipping' to specified truncation values, using in-house software to filter the pseudoseam data. Filtering can be by throw, trace maximum throw, trace length, orientation, quality flag or by combinations of these criteria. The maps and results presented are all based on throw filtering which removes fault traces, or parts of fault traces, which have throws of less than the truncation value specified. The clipping algorithm uses linear interpolation between digitized throw values to select the point at which a fault trace is to be terminated.

Truncated maps with fault throws clipped at 0.6, 1, 5, 10, 20 and 40 m are shown in Fig. 6 and illustrate the profound effects of truncation on a fault data set. Throws below 0.6 m are believed to be incompletely represented on the primary pseudoseam map (see below) and the 0.6 m map is therefore the least truncated valid fault map which is available for this area. A valid map is defined as one in which the geological structures shown, faults in this case, are completely represented above a known size limit and on which no structure below this limit is represented. Statistical analysis of an invalid map, e.g. the primary pseudoseam map, would provide results of uncertain status. Any geological map which is to be used for quantitative analysis should have a clearly defined truncation value. The clipped maps shown in Fig. 6 are similar, but not identical, to fault maps which would be derived from seismic data sets with different fault throw resolutions. Differences between clipped and seismic maps arise from the limited lateral resolution of the seismic technique which causes closely spaced faults to be imaged as a single fault. At typical depths for U.K. coal workings the lateral resolution of seismic would be no better than 17 m, so two 3 m throw faults only 17 m apart would be imaged as a single 6 m offset. Our clipping procedure would remove both these faults. A 5 m throw resolution 'pseudoseismic' map based on a lateral resolution of 17 m has been prepared manually and compared with the automatically clipped 5 m map. The differences between the two maps are small and insignificant for most purposes. Differences would be greater for clipping values <5 m, but for clipping values >5 m the differences would be undetectable and the clipped maps can be regarded as 'pseudoseismic' maps. Even for resolutions which are typical of good quality seismic data from North Sea reservoirs (i.e. vertical resolution—20 m, lateral resolution—50 m) the differences between the fault pattern on a clipped map (Fig. 6e) and its corresponding pseudoseismic map would not be significant: this would not necessarily be the case for other fault systems with different population systematics and spatial distributions.

Most fault data for new developments in coal mining and for hydrocarbon reservoir development are derived from seismic surveys and the clipped versions of the primary map illustrate some of the problems associated with seismic data. Planning for longwall mining should,

Fig. 6. (a)–(f) Clipped versions of the primary map with clipping values of 0.6, 1.0, 5.0, 10.0, 20.0 and 40.0 m. Those parts of fault traces wih throw values less than the clipping value have been deleted. Note the relatively greater reduction of NW fault traces at clipping values on 20.0 and 40.0 m clipped maps.

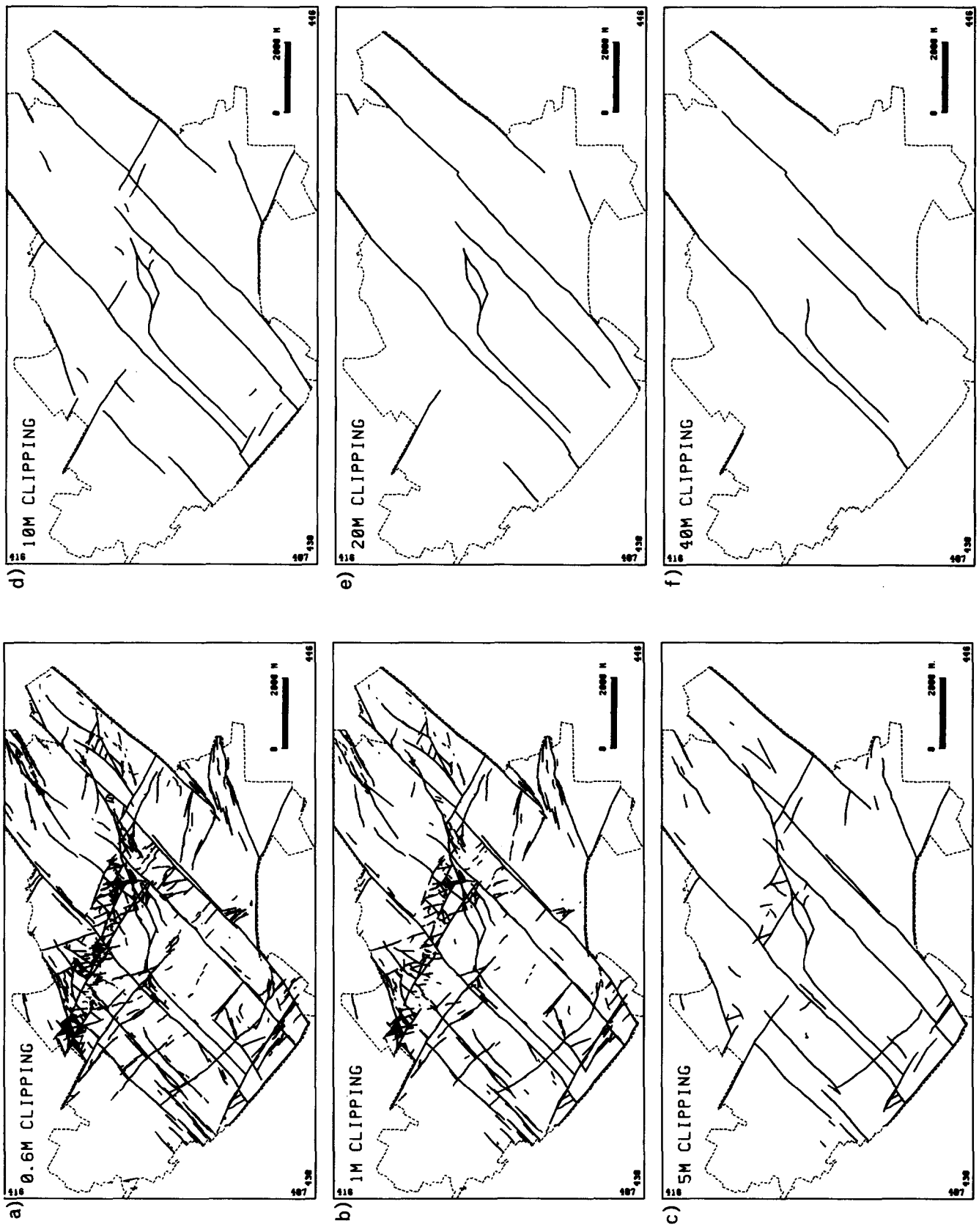
a) 0.6M CLIPPING
b) 1M CLIPPING
c) 5M CLIPPING
d) 10M CLIPPING
e) 20M CLIPPING
f) 40M CLIPPING

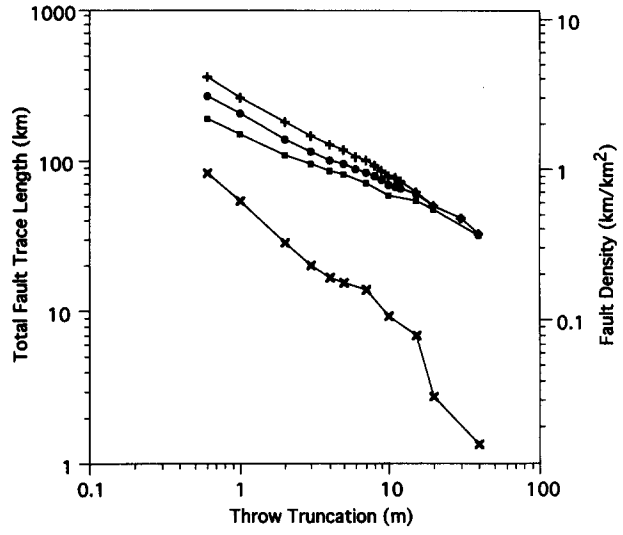

Fig. 7. Variation of fault trace density (and total fault trace length) with clipping value for the mapped area. Note that fault trace density values have meaning only in the context of specified truncation values. Curves are shown for the complete data set (+), for the complete dataset with strike-slip fault zones deleted (solid circles), for the NE normal fault set (solid squares) and for the NW normal fault set (cross). Curve slopes are given in Table 3.

ideally, be on the basis of a map with a truncation value no greater than 1.0 m, i.e. the maximum seam offset which does not seriously disrupt operations. As the very best truncation value obtainable from a surface seismic survey is no lower than 5 m, comparison of the 1 and 5 m clipped maps demonstrates the degree to which a seismically derived fault map would be inadequate for identifying rectangular longwall panels free of faults with throws >1.0 m. The area of the map is similar to those of large North Sea reservoirs and is, in some respects, a good analogue of a faulted reservoir. At depths typical for North Sea reservoirs, the best vertical resolution likely to be achieved by seismic reflection is *ca* 20 m and a more typical value would be closer to 40 m represented, respectively, by the 20 and 40 m clipped maps. These maps show little evidence of the NW normal fault set and nothing of the Holgate Hospital and North Gawber strike-slip zones.

The fault densities (trace length/area) for a range of truncation values are shown in Fig. 7 from which it is evident that 'fault density' is a meaningless attribute unless a truncation limit is specified. The data in Fig. 7 define almost straight lines but the NW fault set curve is irregular (see Table 3 for slopes). The fault density of the mapped area at a truncation value of 40 m, is 0.4 km km^{-2} which falls within the range of fault densities of typical faulted North Sea reservoirs (0.2–2.0 km km^{-2}), for the same truncation value.

An important question concerns the extent to which valid predictions of 'sub-truncation value' faults can be made, either from the various clipped maps or from equivalent seismically derived maps. This paper is concerned only with the densities and size distributions of seismic and sub-seismic faults and with the true lateral extents of seismically imaged faults; questions concerning the spatial distribution of faults will be considered elsewhere.

FAULT POPULATION STUDIES

In recent years many authors have suggested that the size populations of faults are described by power-law distributions (Kakimi 1980, Childs *et al.* 1990, Marrett & Allmendinger 1991, Walsh *et al.* 1991, Jackson & Sanderson 1992, Yielding *et al.* 1992, Scholz *et al.* 1993), where size is expressed either as displacement or dimension. This relationship can be expressed as

$$N \propto S^{-C}$$

where N is the number of faults of size greater than or equal to S and C is the power-law exponent. When this function is plotted on log–log axes, a straight line results with a slope of $-C$. Fault systems are generally analysed from either line samples (one-dimensional) or maps (two-dimensional). One-dimensional displacement populations are derived by recording fault displacements (d) or throws, at the points of intersection between fault traces and an array of, generally fault-perpendicular, parallel sample lines. Two-dimensional fault populations represent either the maximum displacement (D) or the trace length (L) of individual fault traces intersecting a given horizon. The interrelationship between population exponents of displacement ($-C_d$), maximum displacement ($-C_D$) or trace length ($-C_L$) populations (Marrett & Allmendinger 1991) is dependent on the relationship between maximum displacement (D) and fault length (L),

$$D \propto L^n \quad (1)$$

such that

$$C_L/C_D = n \quad (2)$$

and

$$C_d = C_D - 1/n. \quad (3)$$

The above expressions are valid only when the spatial distributions of faults show no lateral or vertical bias with respect to either the sample lines (one dimension) or the sample horizon (two dimensions) (Weibel 1979, Marrett & Allmendinger 1991). The throw truncation method we use provides an unbiased one-dimensional population and no systematic vertical bias is evident from fault maps of different seams.

Populations from a variety of fault systems provide a range of C values, with, for example, line sample displacement populations having C_d within the range 0.4–1.0 (Yielding *et al.* 1992, Gillespie *et al.* 1993, Pickering *et al.* 1994, Nicol *et al.* 1996). The power-law nature of fault size distributions suggests that fault systems are in some respects self-similar and provides a basis for both quantitative definition of the fault size scaling law and for prediction beyond the limits of the data. However, only in a few cases (Walsh *et al.* 1991, Yielding *et al.* 1992, Scholz *et al.* 1993) has the power-law size distri-

Table 3. Slopes of population curves for different sample types for NE and NW normal fault sets and for NE and NW sets combined. The values derived from density vs clipped value plots (Fig. 7) are classified as one-dimensional even though derived from two-dimensional data because the exponents are equivalent to those for one-dimensional samples. The mean and range of slope values are for the visual best-fit lines constructed by five individuals. The range reflects the sometimes subjective judgement of what parts of the tails of the population distribution are incorporated in the best-fit line: this subjectivity would also apply to least-squares regression analysis. Slopes of trace length population curves are, as described in text, minimum values only

Sample type	Figure No.	NE set	NW set	NE + NW
One-dimensional density (km km^{-2})	7	−0.40 ± 0.03	−0.96 ± 0.08	−0.47 ± 0.03
One-dimensional throws	8	−0.54 ± 0.02	−0.82 ± 0.06	−0.69 ± 0.05
Two-dimensional max throws	9	−1.10 ± 0.1	−1.53 ± 0.05	−1.14 ± 0.07
Two-dimensional trace lengths	10	−1.36 ± 0.06	−1.87 ± 0.16	−1.52 ± 0.09

bution of faults in a given data set been tested over more than 2 orders of magnitude: even in these cases, testing required comparison of population curves for different fault size range subsets of the primary data sets. The South Yorkshire data set covers a range of fault size of *ca* 2.5 orders of magnitude with more faults than other individual data sets and therefore provides a firm basis for testing the power-law size distribution of a fault system. The principal objectives of fault size population characterization are: (i) to determine the resolution of the primary pseudoseam map; (ii) to determine the scaling systematics of the fault population; and (iii) to determine whether or not the fault size population of, say, the 1 m clipped map can be derived by analysis of, say, the 5 m clipped map.

POPULATIONS—ONE-DIMENSIONAL SAMPLING

The principal directions of the NE- and NW-striking normal fault sets are *ca* 055° and *ca* 140°, respectively (Fig. 5). The two dominant directions are well-defined on strike histograms, and are also evident by inspection of the maps (Fig. 2): because smaller faults have more variable strikes the distinction between the dominant directions is clearer when the contribution of individual fault traces is weighted by either fault trace length or maximum throw (Figs. 5c & d). The entire population of normal faults can therefore realistically be considered as the sum of the two fault sets. The one-dimensional fault throw population can therefore be sampled adequately using only two sampling directions, one for each set, and the sample line directions used are approximately orthogonal to the respective fault sets. Faults associated with the Holgate Hospital and North Gawber strike-slip zones are excluded from most of the fault size analyses.

Two sampling line directions, 044° and 137° were chosen with some sample lines staggered to avoid areas of incomplete data (Fig. 3). Sample lines are spaced at *ca* 2.0 km and the five NE lines and six NW lines range from 2.7 to 11.8 km in length. At each intersection of a sample line with a fault trace, the distance from the line origin, the fault throw, and the fault strike and dip directions were recorded. Fault throws at the sample points were determined by linear interpolation between the nearest throw values.

The single line throw populations (Walsh *et al.* 1991, Jackson & Sanderson 1992, Yielding *et al.* 1992) derived from the primary map mostly have too few data points for reliable definition of a fault population (see Table 2) and even those with >30 data points are irregular (Fig. 8a). Line NW3, which samples the NE-striking fault set,

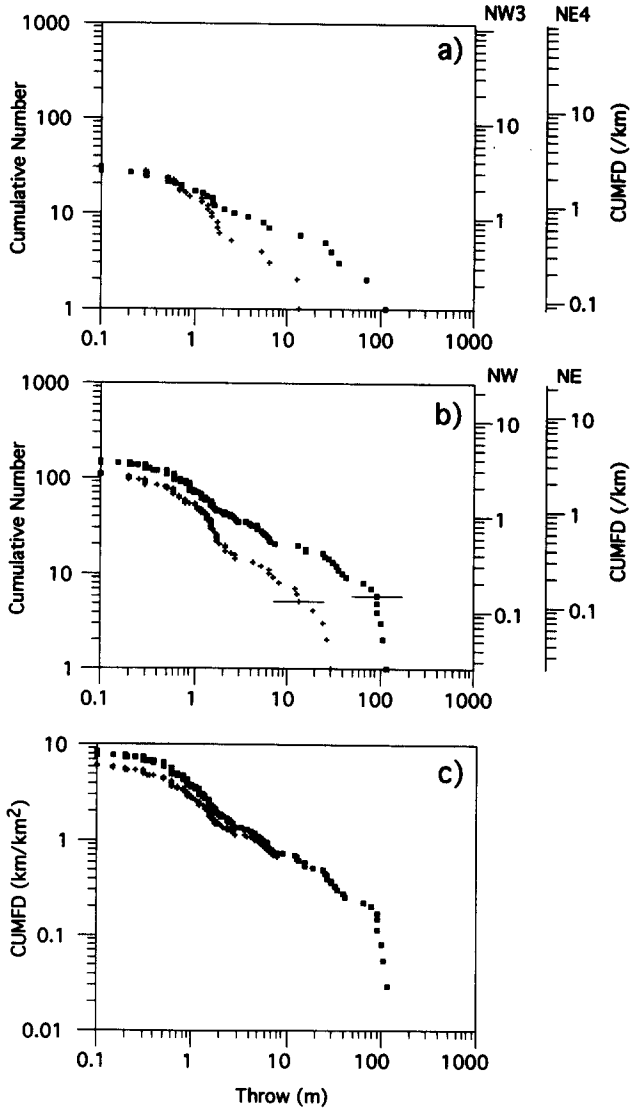

Fig. 8. Throw populations for line samples. (a) Single lines—all traces intersected by sample line NW3 (+) and sample line NE4 (filled squares). (b) Multi-line samples of NE-striking fault set (+) and NW-striking faults (filled squares). Multi-line curves have steep tails at higher throw values up to cumulative numbers approximately equal to number of sample lines, shown by horizontal bars. (c) Multi-line samples of all fault trace data (filled squares) and with strike-slip zones omitted (crosses).

gives a slope of *ca* −0.46 for throw values >50 cm. The data for line NE4, which samples the NW-striking fault set, are irregular and have a smaller throw range than NW3; although the slope is very poorly defined, it is estimated to be *ca* −0.8 and distinctly steeper than the slope for NW3.

Throw population plots for multi-line samples (Yielding *et al.* 1992) of each fault set are shown in Fig. 8(b) (see Table 3 for slopes). Both populations show the three segments characteristic of multi-line plots. Steep right-hand segments have lengths corresponding approximately to the number of lines included in the sample; in each case the number of sample lines is indicated by a short horizontal line (Fig. 8b). The shallow left-hand segments represent throw values which are incompletely sampled and the junction of these segments with the central segments define the truncation values; the truncation value for both fault sets is 60 cm. The central segment is, in ideal cases, straight and the slope and position of this segment characterizes the throw population; extrapolation of this segment allows an estimate to be made of the numbers of fault throws with values less than the truncation value. The central segments of the curves in Fig. 8(b) both have pronounced irregularities which are attributed to data concentrations due to rounding at 100 ft (30.48 m) and 10 m, with inflections at 2–3 m possibly due to rounding to 10 ft but more likely because this is the boundary between throw values derived by direct measurement and those derived from offsets of depth contours. The relative accuracy and the completeness of throw data derived from depth contours are expected to be least satisfactory for throws which are small relative to the contour spacing, and undersampling of the smaller contour-derived throw values has probably occurred. Despite the irregularities, the slope for the NE fault set, *ca* −0.54 is clearly lower than that for the NW fault set which is *ca* −0.82 (Table 3). It is evident by inspection of the curve for the NE fault set that extrapolation from a data set containing only throw values ≥10 m would provide a reasonable estimate of the ≥1 m throw population. On the other hand, a comparable estimate for the NW fault set would require a data set with a truncation value no higher than 5 m. In both cases the estimates would be of low confidence because of the irregularities of the central segments of the curves. The benefit of separating the two sets for plotting and analysis is emphasized by their combined population plot (Fig. 8c). Although perhaps more regular than either of the constituent curves, the combined population curve has a slope, estimated at *ca* −0.69 (Table 3), about midway between that of the individual slopes even though the NW fault set data are fewer than those for the NE set.

The population curves for the NE and NW fault sets converge at a throw of *ca* 20 cm indicating that at a resolution of *ca* 20 cm the one-dimensional fracture densities of the two faults sets would be the same, *ca* 3 faults km^{-1} (Fig. 8b). Fault density values can be misleading, not only when maps with different or poorly defined truncation values are compared but also when size populations with different power-law slopes are compared. As fracture densities represent fault trace lengths per unit area they are only indirectly related to fault-related strain. A better indication of the relative contributions of the two fault sets to the regional extensional strain is given by the aggregate throw km^{-1} sample line length, for a given range of throws. The NE fault set has a throw of 34.4 m km^{-1} for throws ≥60 cm, averaged over all NW sample lines, and the NW fault set a mean throw of 6.0 m km^{-1}, corresponding to β values of 1.013 and 1.002, respectively (assuming fault dips of 70°).

Plots of throw truncation value vs cumulative trace length provide an alternative method of characterizing a fault throw population (Fig. 7). Although derived from map data, these curves sample fault throws, a one-dimensional fault attribute, and their slopes (see Table 3) have a significance identical to that of throw population curves which have previously been regarded as the only way of measuring the one-dimensional population exponent. In both types of plot, the y axis values are directly proportional to fault density (km km^{-2}) and the x axis values are equivalent to throw truncations. Furthermore, because throw truncation curves incorporate all fault trace data, being equivalent to line samples with sample line spacing of zero, they provide a more accurate representation of the one-dimensional throw population and a more continuous type of sampling than throw measurements on discrete sample lines. The slopes of throw truncation vs trace length curves are similar to those of one-dimensional throw population curves, i.e. −0.40 for the NE-striking fault set and −0.96 for the NW-striking set (Fig. 7 and Table 3).

POPULATIONS—TWO-DIMENSIONAL SAMPLING

Two-dimensional sampling measures properties of the map fault trace population. *Fault trace maximum throw* sampling provides the population of maximum throws as recorded on each fault trace in the map area: these throws are unlikely to be the maximum throws on the three-dimensional fault surfaces. *Fault trace length* sampling gives the population of lengths of all fault traces in the map area.

Fault trace maximum throw populations

The maximum throw populations for the NE- and NW-striking fault sets and for their combined population are shown in Figs. 9(a)–(c): their slopes are *ca* −1.10 (NE and combined) and *ca* −1.53 (NW; Table 3). Straight segments spanning *ca* 2 decades of maximum throw are better defined than those for the one-dimensional populations in spite of prominent irregularities due to rounding at 10 and 100 m. Truncation values estimated from the population curves are 60 cm. It is apparent from inspection of Figs. 9(a) & (c) that a good estimate of the 1 m maximum throw populations

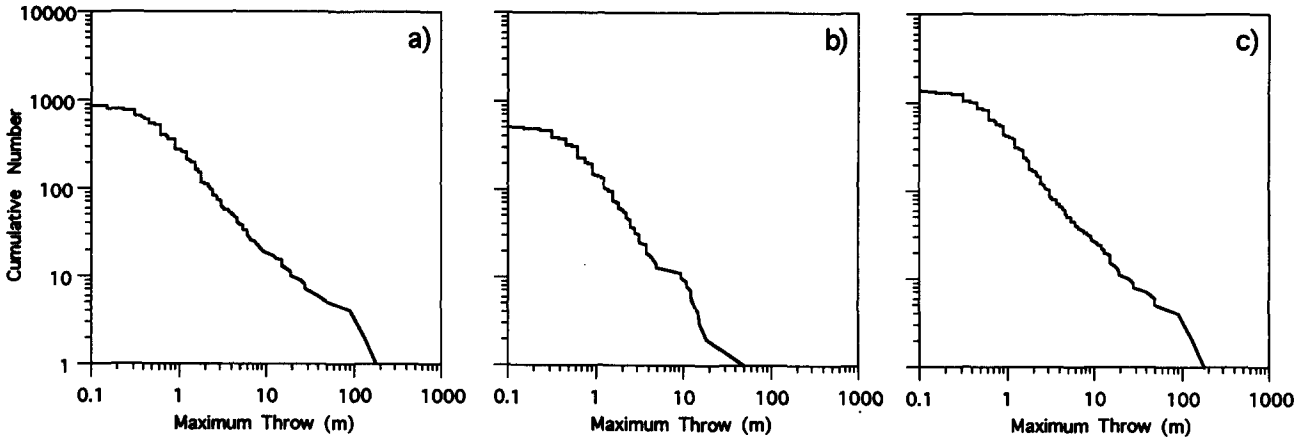

Fig. 9. Trace maximum throw populations for: (a) NE-striking fault set; (b) NW-striking fault set; and (c) NE and NW sets combined.

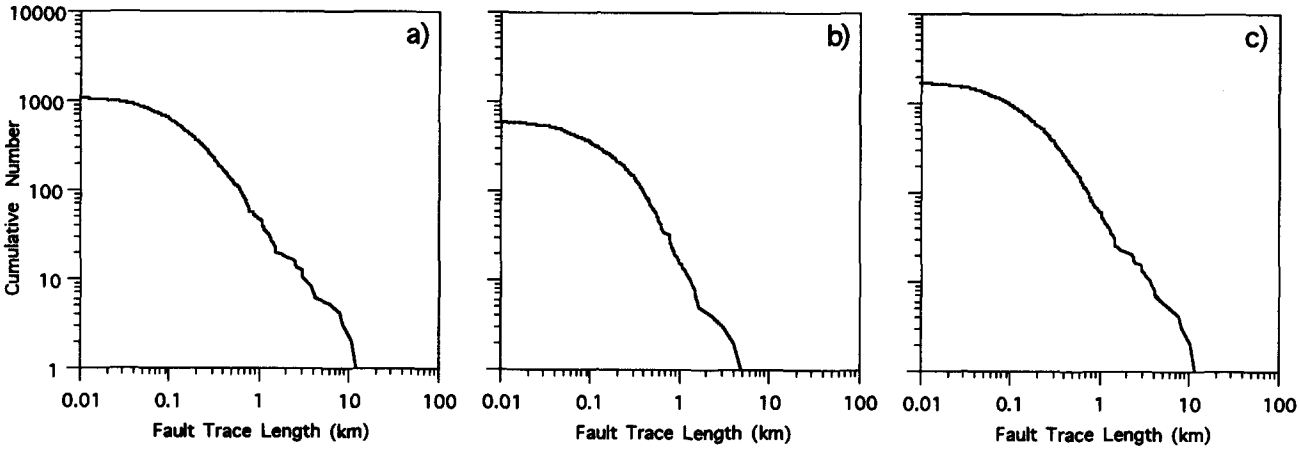

Fig. 10. Trace length populations for: (a) NE-striking fault set; (b) NW-striking fault set; and (c) NE and NW sets combined.

could be obtained for both the NE and the combined data sets by extrapolation from data sets containing only traces with throws $\geq$10 m. A data set with a truncation limit of $\leq$*ca* 2.5 m would be required to make a comparable estimate for the NW fault set (Fig. 9b).

Fault trace length populations

Fault trace length populations are shown in Fig. 10, and it is clear that the curves are different from those for throw and maximum throw populations and have relatively short straight central segments. It is known that length data are affected both by censoring and truncation effects (Heffer & Bevan 1990). Truncation causes the curves to shallow at small length values in the same way as for throw populations (Figs. 10a–c). Censoring refers to the intersection of some fault traces (fault surfaces in three dimensions) with the boundary of the sampled area (volume in three dimensions) so that their true lengths are not represented on the map. Censoring is not of great significance unless the sample area is small relative to the full lengths of most of the fault traces (see Heffer & Bevan 1990, Yielding *et al.* 1992).

The trace length population curves for the NE and NW sets and for their combined population (Figs. 10a–c) have well-defined straight segments spanning, with only minor irregularities, 1.2 decades of trace length; slopes are *ca* −1.36 (NE), −1.52 (combined) and −1.87 (NW; Table 3). Truncation values are *ca* 200 m, with that for the NW faults slightly higher at *ca* 250 m. The highest trace length value within the straight segment of the curve for the NE faults is *ca* 5 km which represents the maximum trace length not strongly affected by censoring (Figs. 10a–c). Five kilometres is about 50% of the map dimension in a NE direction. The corresponding value for the NW fault set is 1.5 km which is much less than the map dimension but is similar to the typical spacing between large NE faults; NW faults often abut against NE faults. Consequently, the population curve for the combined data set has a slightly concave upwards form with a steeper slope than that of the NE fault set but does not allow the two quite distinct populations of the NE and NW fault sets to be distinguished: this feature illustrates the importance of analysing fault sets separately.

Although the effects of throw truncation on both throw and maximum throw population data can be seen simply by inspection of the population curves, the effects of throw truncation on trace length populations are more subtle. Throw truncation effects on fault trace length populations were investigated by plotting trace length populations for a range of clipped maps for the

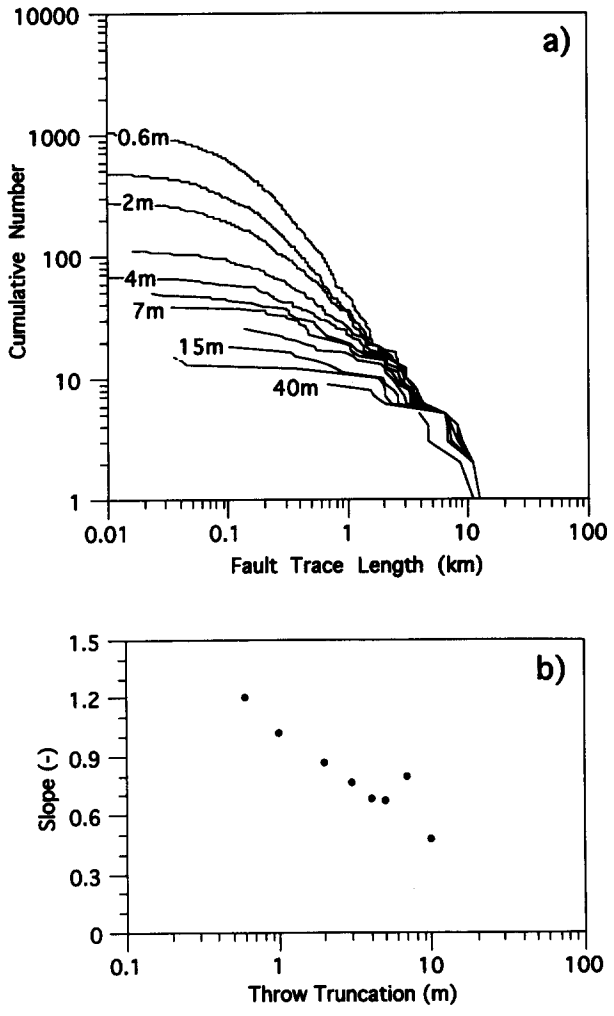

Fig. 11. (a) NE-striking fault set trace length populations for the primary map and for maps clipped at 0.6, 1, 2, 3, 4, 5, 7, 10, 15, 20 and 40 m. (b) Slopes of trace length population curves in (a). Slopes for throw truncation values greater than 3 m are poorly defined. The slope of the unfiltered primary map curve (i.e. −1.36) is not plotted because a well-defined throw truncation value does not apply.

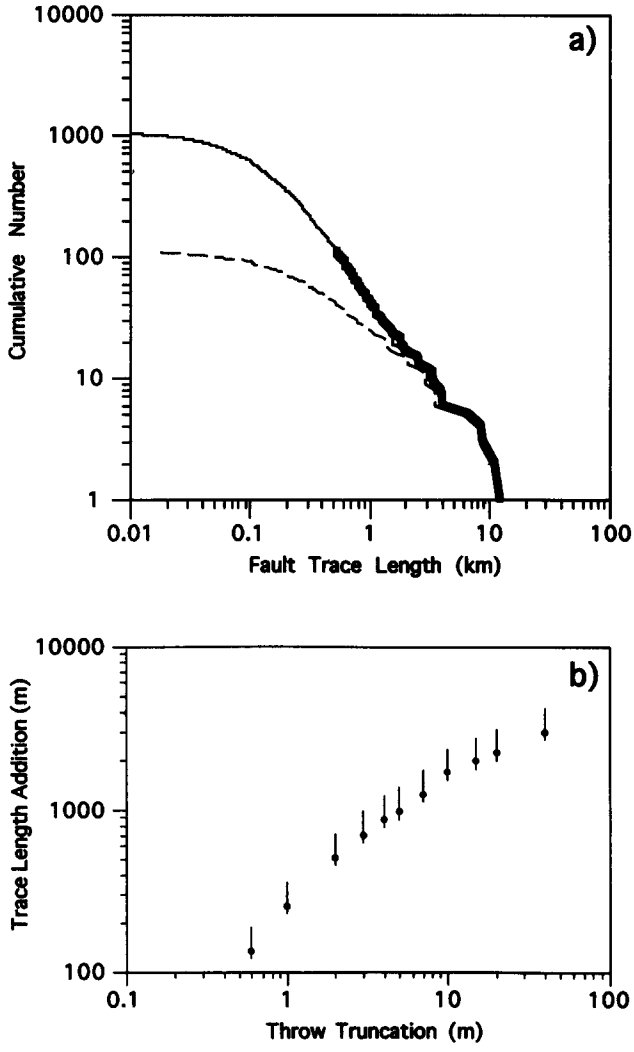

Fig. 12. (a) NE-striking fault set trace length populations for the primary map (solid line) and 3 m clipped map (broken line) and the restored curve (heavy solid line) obtained by adding 700 m to all trace lengths on the 3 m clipped map. (b) Trace length additions required to restore NE fault set trace length population curves for clipped maps to the primary map curve. Vertical bars show maximum ranges of uncertainty.

NE-striking fault set (Fig. 11a). This fault set was chosen for analysis because it is the main normal fault set and because the NW fault set often abuts against and is compartmentalized by NE-striking faults. Truncation has a marked effect not only on the form but also on the slope of a trace length population curve. Slopes decrease with increasing truncation and, taking account of the irregular 'censoring tail', a straight segment is either poorly defined or absent when the throw truncation value is $\geqslant 3$ m (Fig. 7). The value of 3 m is specific to this data set in which the censoring effect begins at 5 km trace length; these values determine the upper and lower bounds of a possible straight line segment of the population curve.

The degradation of trace length population curves with increasing truncation means that valid extrapolation of the curves to lower truncation values is not possible. This is a crucial difference between trace length populations and throw and maximum throw populations. However, a plot of trace length population slope vs throw truncation for the NE-striking fault set shows that trace length population slopes are not converging rapidly at lower truncation values (Fig. 11b), suggesting that at throw truncations of 0.1 m the length population slope may be <-1.5, whereas at truncations of 0.6 m the slope is *ca* −1.20 and is *ca* −1.36 for the unfiltered fault data. Trace length populations derived from truncated data sets will always provide population curves which are shallower than those for untruncated data sets. However, throw truncation and the plotting of population slope vs throw truncation provide a reasonable basis for estimation of the untruncated trace length population slope.

The relationship between throw truncation and fault trace length populations can be explored further using a simple restoration procedure for degraded trace length curves. Taking the primary map trace length population curve for the NE-striking fault set as the closest available to an untruncated data set, each degraded curve can be restored to coincide with the primary map curve by adding a constant length to every trace length in each clipped data set (Fig. 12a). The additional lengths

required at each clipping value are shown in Fig. 12(b). The added lengths required to match curves are subject to some uncertainty as the curve matching is subjective, but the differences between values obtained independently by two people are insignificant. Figure 12(a) shows the effects of adding 700 m to every trace length in the 3 m clipped data set. This restoration is consistent with the 3 m truncation removing 350 m of trace length at each tip point on the original map, but this is unlikely to have occurred. The added length value required to achieve a satisfactory restoration is, in practice, only a good estimate of the average value required to restore the smallest, and most numerous, trace lengths. Although the added length value is large relative to the smallest trace lengths it represents only a small proportion of the larger trace lengths. Given an initial power-law distribution, or similar, a visually satisfactory log–log curve restoration for the longer trace lengths can be obtained even when the added length value for the longer traces in a data set is incorrect by a factor of as much as 10 times. Thus the added trace lengths for each clipping value are valid for only the smallest fault traces in each data set.

The additional length required at each clipping value is plotted in Fig. 12(b) together with the estimated ranges of uncertainty. Given that the throw clipping procedure involves no consideration of length and is executed solely on the basis of interpolation between measured throw values, the plot demonstrates a systematic relationship between trace additional lengths and clipping values. The principal conclusion to be drawn is that the trace length removed per metre of clipped throw increases non-linearly with increase in truncation value, and therefore that throw gradients increase systematically with increasing fault trace length. This relationship is consistent with a non-linear relationship between the maximum displacement on a fault trace (D) and fault trace length (L) as described later.

RELATIONSHIP BETWEEN MAXIMUM THROW AND FAULT TRACE LENGTH

The relationship between maximum displacements and maximum dimensions of faults has been investigated by several authors (e.g. Marrett & Allmendinger 1991, Cowie & Scholz 1992, Gillespie *et al.* 1992, Dawers *et al.* 1993) and no consensus has been reached other than that a power-law relationship exists, which can be expressed as

$$D \propto L^n, \quad \text{where } 1 \leqslant n \leqslant 2.$$

This relationship can be established for data sets which include only tip-to-tip faults which do not bound relay zones: incorporation of other faults is geologically indiscriminate and introduces additional scatter to the data. Plots of log (maximum throw) vs log (trace length) for all fault traces and for tip-to-tip fault traces of the NE fault set are shown in Figs. 13(a) & (b): the NW fault set is excluded from the analysis because fault traces are often restricted by and abut against the NE-striking faults. The bands of data have widths of *ca* 2 decades of trace length, which is more than can be accounted for by variations due to fault traces representing chords on elliptical fault surfaces (Walsh & Watterson 1988a,b, Cowie & Scholz 1992) but the data distributions are consistent with n being equal to, or possibly greater than, 1.0. Many of the mapped fault traces from the data set have only one zero throw tip-point due either to censoring at the map boundary or because they abut against or splay from other fault traces. To allow comparison with displacement–dimension fault data from other sources (Marrett & Allmendinger 1991, Cowie & Scholz 1992, Gillespie *et al.* 1992) these fault traces (censored, abutting and splaying faults) are excluded in Fig. 13(b). This subset still however includes faults which bound relay zones, a factor which introduces significant scatter to the distribution (Gillespie *et al.* 1992, Cartwright *et al.* 1995, Dawers & Anders 1995). We have not however excluded relay-bounding fault traces because they can not be identified objectively in this data set. Although the displacement data are good enough for some purposes they can not identify different degrees of interaction, and therefore displacement transfer, between all faults (see Huggins *et al.* 1995).

Truncation effects need to be considered in all studies of displacement–dimension data. Where fault data are derived from either a single source or by a single imaging technique, faults of all sizes will have similar truncation values. Our analysis of clipped data sets, which reproduce the effects of throw truncation (Figs. 11 and 12), shows that truncation has a proportionally greater effect on the fault trace lengths of smaller displacement faults. Truncation will therefore result in some distortion of the data distribution on log D vs log L plots, so that the slope of the distribution in Fig. 13(b) represents a minimum value for the exponent n in the displacement–dimension relationship. In data sets which include a wide range of fault sizes from varied sources, truncations will tend to be proportional to fault size resulting only in minor translation of the data field with no distortion.

The effects of variable truncation values are removed in Fig. 13(d), which is derived from a tip-to-tip version of the 0.6 m clipped map. As the 0.6 m clipped data set is known to underestimate the lengths of fault traces on the unclipped data set by an average of 135 m (Fig. 12b), this amount has been added to all trace lengths to produce Fig. 13(e), significantly changing the distribution of data points. Given that even the primary data set is also affected by truncation, so that an apparent tip-point with a 10 cm throw could occur more than 50 m from a true fault tip-point, an additional *ca* 100 m would need to be added to trace lengths to remove entirely truncation effects from both ends of each fault trace. Figure 13(f) shows the effect of adding a total of 235 m to the trace lengths plotted in Fig. 13(b). Insofar as slopes can be assigned to the data distributions in Figs. 13(e) & (f), it is clear that n is either equal to or, in our view, greater than 1. This exercise demonstrates the sensitivity of throw–dimension data to truncation which, if not taken

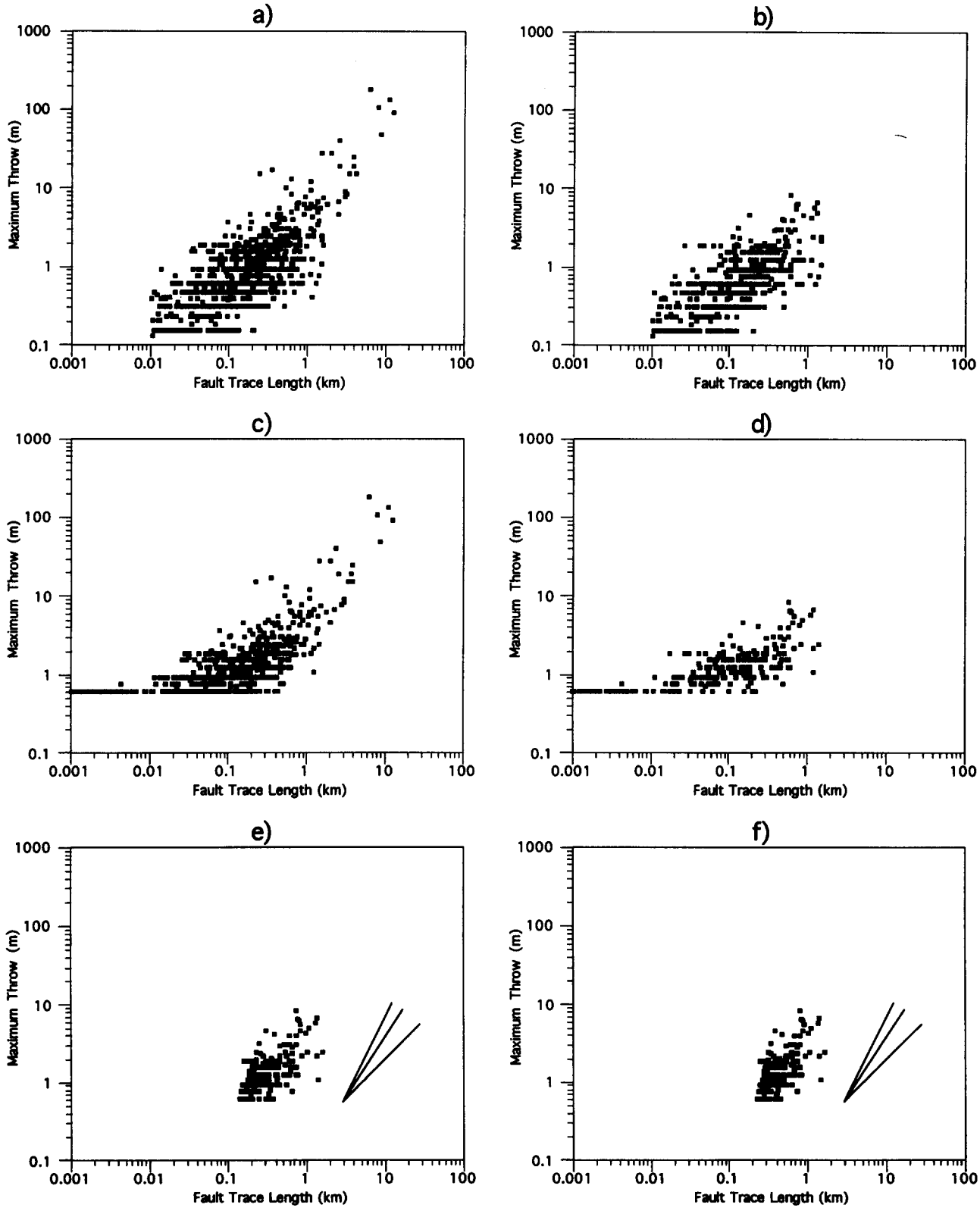

Fig. 13. Trace length vs maximum throw for all NE-striking fault traces (a & c) and for NE-striking fault traces terminated by two tip-points (tip-to-tip traces) including those bounding relay zones (b,d–f). (a) & (b) Primary map; (c) & (d) 0.6 m throw clipped map; (e) 0.6 m throw clipped map with 135 m added to each trace length; (f) 0.6 m throw clipped map with 235 m added to each trace length. Compensation for truncation changes the data distributions and the ranges of probable slopes of the bands of data points. Lines on (e) and (f) have slopes of 1, 1.5 and 2.

into account, can distort data distributions and give rise to estimates for the value of n which are significantly lower than the true value.

Because of the difficulty of assigning slopes to D vs L scatter plots (Fig. 13), comparison of the slopes of well-defined power-law size distributions (i.e. maximum throw and fault trace length) provides a potentially more robust method for determining the D vs L relationship

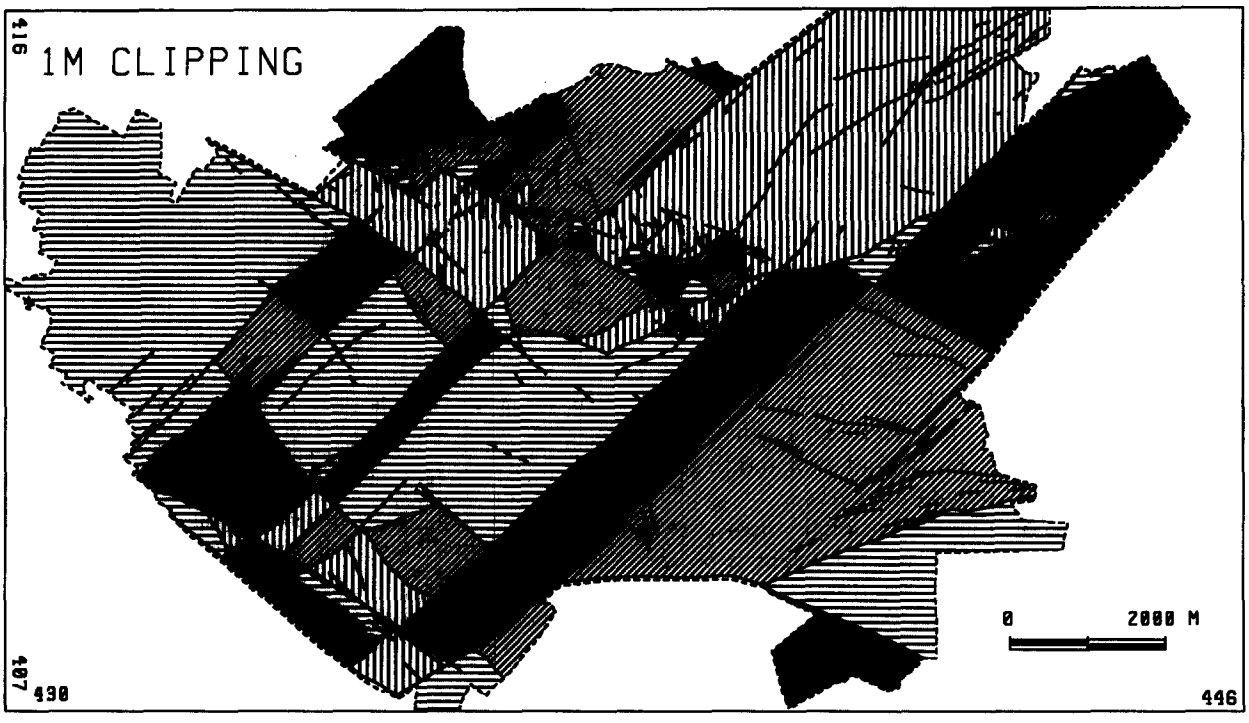

Fig. 14. Primary map clipped at 1 m throw showing 54 separate fault compartments.

(equation 2). As this method is still subject to truncation effects only a minimum value for n can be obtained. The main NE-striking fault set and the combined normal fault data set each provide a value for C_L/C_D greater than 1.25.

COMPARISON OF THE DIFFERENT TYPES OF POPULATION

The exponents of the three different types of fault size population should be systematically related to one another (Marrett & Allmendinger 1991, Yielding *et al.* 1992), as shown by equations (1)–(3). For the main NE-striking fault set, taking the exponent of throw truncation curves as a more robust measure of the one-dimensional throw population curve, the exponents of one-dimensional throw and two-dimensional maximum throw curves are indicative of $n > 1.25$ with n closer to 1.4. For internal consistency these values require a trace length population exponent, C_L, greater than *ca* 1.5. Figure 11(b) shows that by accounting for the effects of throw truncation, $C_L > 1.5$ is plausible.

APPLICATIONS

Fault size population systematics can be applied to prediction of size population characteristics beyond the size range of the data. The principal application is in prediction of populations of sub-seismic faults from seismic data for hydrocarbon reservoir characterization. Truncation effects are simply identified in the case of throw and maximum throw populations but distort trace length population curves and should be corrected for. Previous work on prediction of sub-seismic faults (Sassi *et al.* 1992, Yielding *et al.* 1992, Gauthier & Lake 1993) has concentrated on prediction of the numbers and locations of sub-seismic faults. Little attention has been paid previously to the extent by which traces of seismically-imaged faults should be extended to conform with a specified truncation value. Truncated fault traces interpreted from seismic data will show high displacement gradients adjacent to fault tips and restoration of fault trace lengths may best be achieved by extrapolation of displacement profiles beyond the mapped fault tips. Fault trace length population slopes should always be regarded as minimum values.

In hydrocarbon reservoirs, sub-seismic faults may affect flow either by increasing the tortuosity of flow paths, or by compartmentalizing a reservoir interval. The extent of potential compartmentalization on the 1.0 m clipped map can be gauged from Fig. 14. The degree of compartmentalization is strongly dependent not only on the fault density but also on the fault orientations; compartmentalization is strongly favoured by orthogonal fault sets such as those occurring in South Yorkshire, U.K. Other applications are in the prediction of populations of faults which are larger than those encountered in boreholes drilled for hydrogeological and engineering purposes. Up-scale prediction has to be undertaken with some caution as the largest fault size in a fault system can be determined only by observation.

The likely effects of a fault array, including sub-seismic faults, on coal mining or on fluid flow in a hydrocarbon reservoir, or the hydraulic integrity of a hazardous waste storage facility cannot be assessed without taking account of the spatial distribution systematics of the predicted population of faults. This

aspect of the South Yorkshire fault map will be considered elsewhere.

CONCLUSIONS

(1) Size populations of faults from a large-scale range fault map of a part of the South Yorkshire Coalfield are power-law over *ca* 2.5 orders of magnitude, for faults with maximum throws from 180 m down to 0.6 m.

(2) All fault maps have a throw truncation value below which fault traces are not shown. Truncation effects either completely remove or shorten the lengths of fault traces and are responsible for degradation and shallowing of fault trace length population curves.

(3) The slopes of one-dimensional throw, two-dimensional maximum throw and trace length power-law populations are interrelated and, taking account of the effects of truncation on trace length populations, are internally consistent.

(4) 'Pseudoseismic' maps have been derived which represent the fault maps which would be expected from seismic surveys of varying resolution. At fault throw resolutions of 20 m, or worse, one of the two normal fault sets in the study area would be eliminated. Extrapolation of population curves for a map with 10 m throw resolution provides an accurate estimate of the throw population down to 0.6 m.

Acknowledgments—We thank Steve Graham, formerly of British Coal, for discussions on the structure of the Yorkshire Coalfield and members of the Fault Analysis Group for assistance with data collection and processing. We also thank Nancye Dawers and an anonymous reviewer for helpful reviews. This research was part funded by the European Coal and Steel Commission (contract No. 7220 AF840) and by the CEC JOULE II Hydrocarbons Programme (contract JOU2-CT92-0182).

REFERENCES

Cartwright, J. A., Trudgill, B. & Mansfield, C. S. 1995. Fault growth by segment linkage: an explanation for scatter in maximum displacement and trace length data from Canyonlands Grabens of S.E. Utah. *J. Struct. Geol.* **17**, 1319–1326.

Childs, C., Walsh, J. J. & Watterson, J. 1990. A method for estimation of the density of fault displacements below the limits of seismic resolution in reservoir formations. In: *North Sea Oil and Gas Reservoirs—II* (edited by Buller, A. T., Berg, E., Hjelmeland, O., Kleppe, J., Torsæter, O. & Aasen, J. O.). Graham & Trotman, London, 309–318.

Cowie, P. A. & Scholz, C. H. 1992. Displacement-length scaling relationship for faults: data synthesis and discussion. *J Struct. Geol.* **14**, 1149–1156.

Dawers, N. H. & Anders, M. H. 1995. Displacement-length scaling and fault linkage. *J. Struct. Geol.* **17**, 607–614.

Dawers, N. H., Anders, M. H. & Scholz, C. H. 1993. Growth of normal faults: displacement–length scaling. *Geology* **21**, 1107–1110.

Gauthier, B. D. M. & Lake, S. D. 1993. Probabilistic modelling of faults below the limit of seismic resolution in the Pelican Field, North Sea, offshore U.K. *Bull. Am. Ass. Petrol. Geol.* **77**, 761–777.

Gibson, J. R., Walsh, J. J. & Watterson, J. 1989. Modelling of bed contours and cross-sections adjacent to planar normal faults. *J. Struct. Geol.* **11**, 317–328.

Gillespie, P. A., Walsh, J. J. & Watterson, J. 1992. Limitations of dimension and displacement data from single faults and the consequences for data analysis and interpretation. *J. Struct. Geol.* **14**,1157–1172.

Gillespie, P. A., Howard, C. B., Walsh, J. J. & Watterson, J. 1993. Measurement and characterisation of spatial distributions of fractures. *Tectonophysics* **226**, 113–141.

Goossens, R. F. & Smith, E. G. 1973. The stratigraphy and structure of the upper Coal Measures in the Yorkshire coalfield between Pontefract and south Kirby. *Proc. Yorks. geol. Soc.* **39**, 487–514.

Graham, S. 1988. Structural elements of the Yorkshire Coalfield with particular reference to Selby and the eastern Coal Measures. British Coal, Internal Report.

Heffer, K. J. & Bevan, T. G. 1990. Scaling relationships in natural fractures—data, theory and applications. Society of Petroleum Engineers Paper No. 20981.

Huggins, P., Watterson, J., Walsh, J. J. & Childs, C. 1995. Relay zone geometry and displacement transfer between normal faults recorded in coal-mine plans. *J. Struct. Geol.* **17**, 1741–1755.

Jackson, P. & Sanderson, D. J. 1992. Scaling of fault displacements from the Badajoz-Córdobe shear zone, SW Spain. *Tectonophysics* **210**, 179–190.

Kakimi, T. 1980. Magnitude–frequency relation for displacement of minor faults and its significance in crustal deformation. *Bull. Geol. Surv. Jap.* **31**, 467–487.

Marrett, R. & Allmendinger, R. W. 1991. Estimates of strain due to brittle faulting: sampling of fault populations. *J. Struct. Geol.* **13**, 735–738.

Nicol, A., Walsh, J. J., Watterson, J. & Gillespie, P. A. 1996. Fault size distributions—are they really power law? *J. Struct. Geol.* **18**, 191–197.

Pickering, G., Bull, J. M., Sanderson, D. J. & Harrison, P. V. 1994. Fractal fault displacements: a case study from the Moray Firth, Scotland. In: *Fractals and Dynamic Systems in Geosciences* (edited by Kruhl, J. H.). Springer, Berlin, 105–119.

Rippon, J. H. 1985a. Contoured patterns of the throw and hade of normal faults in the Coal Measures (Westphalian) of north-east Derbyshire. *Proc. Yorks. geol. Soc.* **45**, 147–161.

Rippon, J. H. 1985b. New methods of forecasting the throw and hade of faults in some North Derbyshire Collieries. *Min. Engng* 198–204.

Sassi, W., Livera, S. E. & Caline, B. P. R. 1992. Reservoir compartmentation by faults in Cormorant Block IV, U.K. northern North Sea. In: *Structural and Tectonic Modelling and its Application of Petroleum Geology* (edited by Larsen, R. M., Brekke, H., Larsen, B. T. & Talleraas, E.). *Spec. Pub. Norweg. Petrol. Soc.* **1**, 355–364.

Scholz, C. H., Dawers, N. H., Yu, J. Z., Anders, M. H. & Cowie, P. A. 1993. Fault growth and fault scaling laws: preliminary results. *J. geophys. Res* **98**, 21,951–21,961.

Walsh, J. J. & Watterson, J. 1988a. Dips of normal faults in British Coal Measures and other sedimentary sequences. *J. geol. Soc. Lond.* **145**, 859–873.

Walsh, J. J. & Watterson, J. 1988b. Analysis of the relationship between the displacements and dimensions of faults. *J. Struct Geol.* **10**, 239–247.

Walsh, J. J. & Watterson, J. 1990. New methods of fault projection for coalmine planning. *Proc. Yorks. geol. Soc.* **48**, 209–219.

Walsh, J. J., Watterson, J. & Yielding, G. 1991. The importance of small-scale faulting in regional extension. *Nature* **351**, 391–393.

Weibel, E. R. 1979. *Stereological Methods: Volume* 1, *Practical Methods for Biological Morphometry*. Academic Press, London.

Yielding, G., Walsh, J. J. & Watterson, J. 1992. The prediction of small-scale faulting in reservoirs. *First Break* **10**, 449–460.